Alterations of specific inhibitory circuits of the prefrontal cortex underlie abnormal network activity in a mouse model of Down syndrome

Javier Zorrilla de San Martin[1*], Cristina Donato[1,2], Jérémy Peixoto[1,3], Andrea Aguirre[1], Vikash Choudhary[1], Angela Michela De Stasi[1], Joana Lourenço[1], Marie-Claude Potier[1*] and Alberto Bacci[1*]

Affiliations:
[1] Institut du Cerveau et de la Moelle épinière (ICM), CNRS UMR 7225 – Inserm U1127, Sorbonne Université, Paris, France.
[2] Present address: Luxembourg Centre for Systems Biomedicine, University of Luxembourg, Belvaux, L-4367, Luxembourg.
[3] Present address: Institut Pasteur, Paris.

***Corresponding authors:**
Alberto Bacci: alberto.bacci@icm-institute.org
Marie-Claude Potier: marie-claude.potier@upmc.fr
Javier Zorrilla de San Martin: Javier.zorrilla@icm-institute.org

Acknowledgements:
We thank Vikaas Sohal, Nelson Rebola and Maria del Mar Dierssen Sotos for critically reading this manuscript. We also thank the ICM technical facilities PHENO-ICMICE and iGENSEQ.

This work was supported by "Investissements d'avenir" ANR-10-IAIHU-06, BBT-MOCONET; Agence Nationale de la Recherche (ANR-12-EMMA-0010 ; ANR-13-BSV4-0015-01; ANR-16-CE16-0007-02; ANR-17-CE16-0026-01; ANR-18-CE16-0001-01), Fondation Recherche Médicale (Equipe FRM DEQ20150331684 and EQU201903007860), NARSAD independent investigator grant and Fondation Lejeune (#1790).

Author contributions:
J.Z.S.M., M.C.P and A.B designed the experiments; J.Z.S.M, A.A., J.P. and C.D performed the experiments; J.Z.S.M., C.D., A.A., V.C. and J.P. analyzed the data; A.M.D.S and J.L. helped with *in vivo* recordings; M.C.P and A.B. supervised the project. All authors participated in writing the manuscript.

Abstract

Cognitive deficits in Down syndrome (DS) can originate from cortical over-inhibition, but whether this is due to specific alterations of distinct GABAergic circuits is unknown. In the prefrontal cortex of a DS mouse model, we found specific enhancement of dendritic inhibition and altered excitability of perisomatic inhibitory interneurons. These effects resulted in reduced pyramidal-neuron firing and increased phase locking to cognitive-relevant network oscillations *in vivo*. Our results reveal potential circuit mechanisms underlying cognitive deficits of DS.

Main

Down syndrome (DS) is a condition caused by full or partial trisomy of human chromosome 21, characterized by various physical and neurological features including mild to severe intellectual disability[1]. Individuals with DS present important deficits in cognitive tasks known to depend on the anatomical and functional integrity of the frontal lobe[2]. Importantly, mouse models of DS recapitulate several cognitive deficits of this condition[3,4].

Recovery of behavioral and neurophysiological deficits underlying cognitive impairments using $GABA_A$ receptor blockers led to hypothesize that intellectual deficits in DS are produced by an excessive activity of inhibitory circuits[5,6]. Nonetheless, direct evidence for over-inhibition in DS is lacking. Moreover, given the anatomical, molecular and functional diversity of cortical inhibitory neurons[7], the functional implications of this hypothesis at the network level and the underlying GABAergic circuits involved remain obscure.

To study DS cortical activity and inhibitory circuits, we used Ts65Dn mice (Ts), a well-established mouse model of DS[8]. In order to assess the activity of the medial prefrontal cortex (mPFC) *in vivo*, we performed simultaneous local field potential (LFP) and loose-patch, juxtacellular recordings from putative pyramidal neurons (PNs) to monitor their spiking dynamics related to overall network activity

(Figure 1a). *In vivo* recordings exhibited typical oscillatory activity consisting of UP and DOWN states[9], similar in frequency and duration in Ts mice and their euploid littermates (Eu) (Suppl. Fig. 1). UP states were enriched in γ-band activity (30-100 Hz) and exhibited increased probability of spiking activity[9]
70 (Figure 1a). Juxtacellular recordings from individual mPFC putative PNs revealed a near 50% decrease in the overall spiking rate in Ts mice as compared to their Eu littermates (Figure 1b, Supplementary Table 1) while analysis of LFP power spectral density (PSD) did not show any significant difference (Figure 1c). Interestingly, when we analyzed LFP waveform specifically around periods of neuronal spiking activity (spike-triggered LFP or stLFP), we found that, in both genotypes, average stLFPs were
75 characterized by marked voltage deflections, indicating that spike probability was not randomly distributed but locked to LFP oscillations (Figure 1d). The peak-to-peak amplitude of the stLFP was much larger in Ts than in Eu mice (Figure 1d,e, Supplementary Table 1), and, remarkably, the spectral power of the stLFP was largely increased in Ts mice, selectively in the β-γ-frequency band (Figure 1f, Supplementary Table 2). In order to quantitatively assess whether PN spikes were differently locked
80 to the phase of network oscillations, we measured the pairwise phase consistency (PPC), which is an unbiased parameter to determine the degree of tuning of single-neuron firing to network rhythmic activity of specific frequencies[10,11]. Ts mice exhibited significantly higher PPC values than Eu littermates for frequency bands ranging between 10 and 60 Hz (Figure 1g), thus revealing stronger phase locking selectively with β- and low γ-oscillations. Altogether, these results indicate that in the mPFC of Ts mice
85 PNs fire less but their activity is abnormally more synchronized than in control Eu littermates.

Both reduced firing rate and increased phase locking are consistent with increased activity of inhibitory interneurons[12,13]. Yet, network oscillations in the β- and γ-frequency bands are driven by different interneuron subtypes[10]. It is therefore possible that the aberrant spiking and network activity

observed in Ts mice are due to specific alterations of distinct cortical inhibitory circuits.

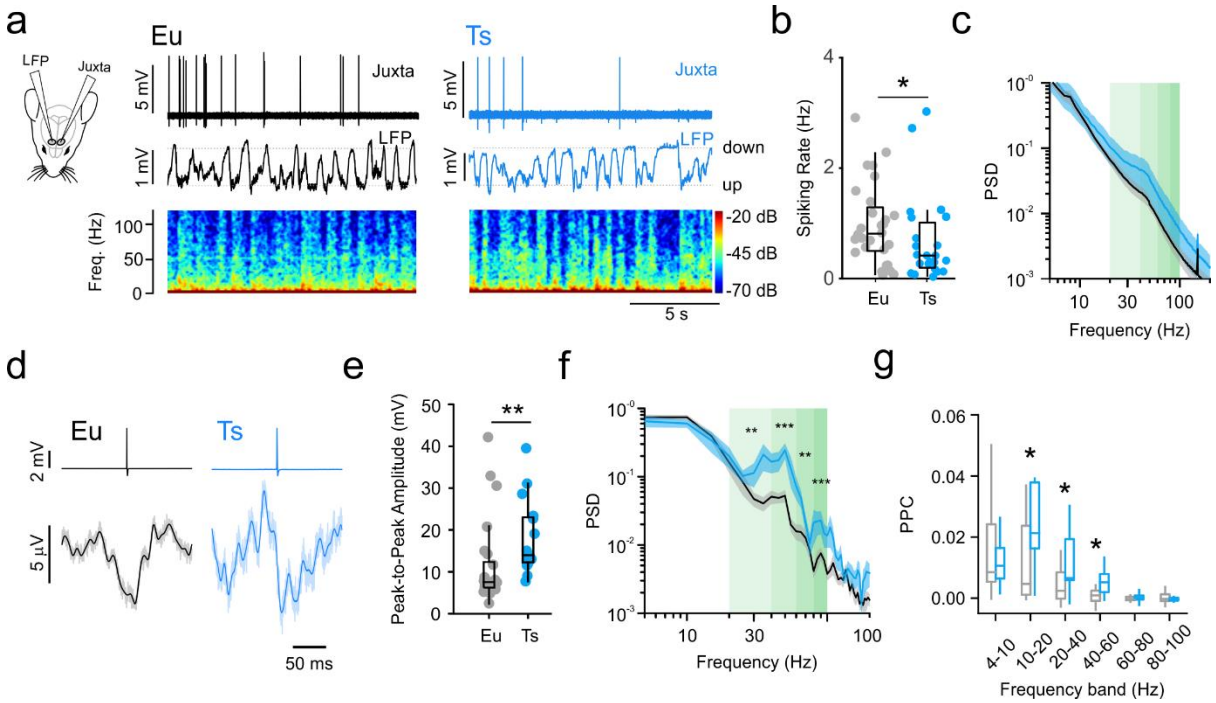

Figure 1: Reduced spiking activity *in vivo* and increased tuning with network oscillations in Ts65Dn mPFC.

a, Left: scheme depicting simultaneous local field potential (LFP) and juxtacellular patch clamp recordings in the mPFC. Right: representative juxtacellular (top trace), LFP (middle trace) and spectrogram (bottom) recorded in Eu (black) and Ts (blue) mice. **b,** Average spiking rate from individual cells. Population data (n=28 cells, 5 mice and 23 cells, 6 mice for Eu and Ts respectively; p=0.03, Mann-Withney U-test). **c,** Power Spectral Density (PSD) from Eu and Ts mice. Shaded green areas correspond to β-γ-frequency ranges. **d,** Representative portions of averaged LFP around aligned spike (spike-triggered LFP or stLFP). Top: Average traces of aligned spikes from a putative layer 2/3 PN recorded in a Eu (black) and Ts (blue) mouse. Bottom: average of the corresponding stLFPs. Light line: raw averaged trace, thick dark line: low pass filtered trace (cutoff: 100Hz). **e,** Average plots of stLFP peak-to-peak amplitude in Eu and Ts mice. **f,** Power spectral density of stLFPs. Shaded green areas correspond to β-γ-frequency ranges. **g,** Pairwise Phase Consistency (PPC) calculated for specific frequency bands (4-10Hz: p=0.427, 10-20Hz: p=0.02145, 20-40Hz: p=0.0418, 40-60Hz: p=0.01638, 60-80Hz: p=0.2308, 80-100Hz: p=0.3161, Mann-Withney U-test). e-g,: n=23 cells, 5 mice and 11 cells, 6 mice for Eu and Ts respectively. Boxplots represent median, percentiles 25 and 75 and whiskers are percentiles 5 and 95. *: $p < 0.05$; **: $p < 0.01$.

In the neocortex, the inhibitory control of dendrites and soma of PNs is operated by a rich diversity of GABAergic interneurons. In particular, somatostatin (SST)-positive Martinotti cells (MCs) are specialized in distal dendritic inhibition, whereas perisomatic inhibition is mostly accomplished by parvalbumin-positive interneurons (PV-INs)[7]. While dendritic inhibition from MCs modulates the integration of long-range synaptic inputs in cortical layer 1 (L1), perisomatic inhibition by PV-INs

shapes the temporal dynamics of spiking output of PNs. Both forms of inhibition were shown to be involved in the entrainment of network oscillations[10,12,13] and in the cognitive performance during mPFC-dependent tasks[14–16].

In particular, inhibition from SST-INs plays a crucial role in mPFC-dependent memory[16]. Interestingly, in the barrel cortex, dendritic synaptic inhibition onto PNs from MCs relies on α5-containing $GABA_A$Rs[17] (recently shown also in their hippocampal counterparts[18,19]). Hence, treatment of Ts mice with selective negative allosteric modulators of α5-containing $GABA_A$Rs reverse cognitive and long-term synaptic plastcity deficits in Ts65Dn mice[19–22]. To test whether dendritic inhibition of PNs by MCs could be affected in Ts mice, we crossed Ts65Dn with GFP-X98 mice, which in the barrel cortex were shown to bias GFP expression in MCs[23]. Accordingly, in these mice, GFP was expressed by a subset of SST-positive interneurons (Suppl. Fig. Figure 2a), exhibiting a widely branched axonal plexus in L1, characteristic of dendrite-targeting inhibitory MCs (Supplementary Figure 2b,c). Using dual whole-cell patch-clamp in acute mPFC slices, we recorded unitary inhibitory postsynaptic currents (uIPSCs) in MC-PN connected pairs and found that dendritic MC-PN synaptic inhibition relied on α5-containing $GABA_A$Rs in both Ts and Eu mice. Indeed, bath application of the selective negative allosteric modulator of α5-containing $GABA_A$Rs, α5IA (100 nM), produced a significant reduction of uIPSCs that was close to the maximal potency of the drug (~40%)[24] in both genotypes (Figure 2a, Supplementary Table 3). Interestingly, MC-mediated uIPSC amplitudes were significantly larger and failure rate significantly smaller in Ts compared to Eu. Moreover, the total amount of charge (Q) transferred during a train of 5 action potentials was near 5-fold larger in Ts than in Eu (Figure 2b). In addition, glutamatergic recruitment of MCs by PNs was also stronger in Ts than Eu mice. Unitary excitatory postsynaptic currents (uEPSCs) in connected PN-MC pairs exhibited larger amplitude, lower failure rate and larger charge transfer in Ts than Eu mice (Figure 2c, Supplementary Table 4). Input-output spiking activity of both PNs and MCs, assessed by injecting increasing depolarizing currents, was similar in Eu and Ts mice (Figure 2d,e; Supplementary Table 5-6). Furthermore, single-action potential features (such as spike threshold, peak and duration), and passive properties (such as input resistance,

resting membrane potential and time constant) were similar in both genotypes (Supplementary Figures 3 and 4; Supplementary Tables 7-8). Importantly, the density of MCs was similar in both genotypes (Figure 2f). Likewise, the spatial distribution and total length of axons and dendrites of both MCs Figure 2g-i) and PNs were similar in Eu and Ts mice (Figure 2j-l).

Altogether, these results indicate a specific synaptic strengthening of the dendritic inhibitory loop involving MCs in Ts mice, suggesting a major impact on PN dendritic integration. Moreover, this synaptic enhancement of the dendritic inhibitory loop in Ts mice could underlie the hyper-synchronization observed *in vivo* (Figure 1). Finally, it highlights a circuit-specific synaptic mechanism underlying the rescue of cognitive deficits in Ts mice, operated by selective pharmacology of α5-$GABA_A$Rs.

Is the synaptic enhancement of the dendritic inhibitory loop involving MCs a specific alteration or a general feature of glutamatergic and GABAergic synapses in Ts mice? To address this question, we measured glutamatergic recruitment onto and synaptic inhibition from another prominent interneuron class, PV basket cells. These interneurons are characterized by their ability of firing at high frequencies, non-adapting trains of fast action potentials. These properties, along with the perisomatic inhibitory basket formed by their axon around the soma of PNs, make PV-INs an efficient regulator of PN output. We thus crossed Ts65Dn with PValbTomato mice, a line that expresses TdTomato specifically in PV-positive INs[25]. We recorded uIPSCs and uEPSCs (Figure 3a-d) from pairs of synaptically connected PNs and PV-INs. The amplitude, failure rate and charge transfer of trains of uIPSCs evoked by action potentials in presynaptic PV-INs were similar in both genotypes (Figure 3a,b; Supplementary Table 9). Likewise, amplitudes, failure rates and charge transfer of uEPSCs elicited by PN firing was indistinguishable in Eu and Ts mice (Figure 3c,d; Supplementary Table 10). Surprisingly, however, we observed major alterations of PV-IN excitability in Ts mice, whose PV-INs required one third less current to fire action potentials, as compared to their Eu littermates. (Figure 3e-g). Moreover, PV-INs in Ts mice could not sustain high-frequency firing in response to 2 s-long

depolarization, and maximal spike rate was thus near half of that reached by PV-INs in Eu mice (Figure 3e-g; Supplementary Table 11).

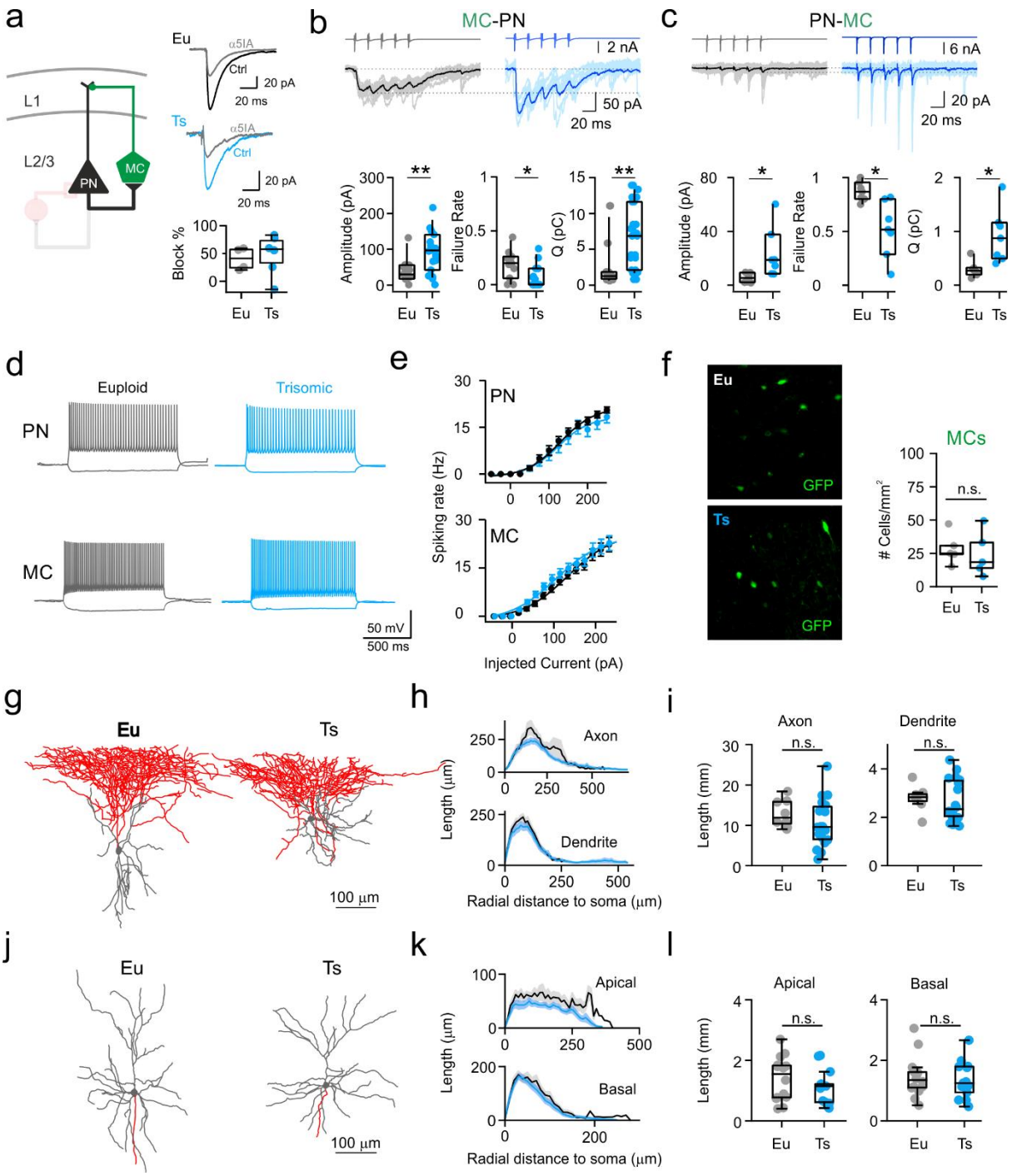

Figure 2: Synaptic enhancement of dendritic inhibition in DS.

a, Left: schematic of the cortical circuit involving PNs and MCs. Right, top: representative voltage-clamp current traces of uIPSCs recorded in a Eu (top) and a Ts (bottom) MC-PN connected pair before (black in Eu and blue in Ts mice) and after (gray) application of the α5-GABA$_A$R inverse agonist α5IA (100 nM). Shown are averages of 50 traces Right, bottom: population data of uIPSC amplitude block by α5IA in Eu and Ts mice. **b,** Top: Representative traces of uIPSCs (lower traces) elicited by a train of 5 presynaptic action currents (50 Hz) to the MC (upper traces).

Eu: individual (gray) and average (black); Ts: individual (light blue) and average (blue) traces. Bottom panels: population data of uIPSC amplitude (p=0.0094, Mann-Withney U-test), failure rate (p=0.0201, Mann-Withney U-test) and total charge transferred during the 5 APs train (Q, p=0.006, Mann-Withney U-test; n=11 and 15 pairs for Eu and Ts respectively). **c,** Same as in **b**, but for glutamatergic uEPSCs triggered by action currents in presynaptic PNs and recorded in postsynaptic MCs (Amplitude: p=0.0398, Mann-Withney U-test; Failure Rate: p=0.0107, Mann-Withney U-test; Q: p=0.0157, Students T-test; n=7 for both, Eu and Ts). **d,** Representative membrane potential responses to current steps of increasing amplitude applied to PNs (left) and MCs (right) from Eu (gray) and Ts (blue) mice. **e,** Spiking frequency as function of injected current. Population data from PNs (left, genotype factor $F_{(1, 598)}$=3.444, p=0.064, two-way ANOVA; n=25 and 23 cells for Eu and Ts correspondingly) and MCs (right, genotype factor $F_{(1, 660)}$=0.004960, p=0.9439, two-way ANOVA; n=26 and 20 cells for Eu and Ts correspondingly). **f,** Quantification of MC somas in the mPFC of Eu and Ts mice. Left: epifluorescence images of immunolabeled GFP in Ts::X98 coronal slices. Right: population data for both Eu and Ts. **g,** Representative reconstruction of biocytin filled L2/3 MCs from Eu and Ts mice. Gray: somatodendritic region, red: axon. **h,** Scholl analysis of MC axonal and dendritic length between concentric circles of increasing radius with 10 µm steps. **i,** Total axonal (left) and dendritic (right) length. **h,i,** n=18 and 8 neurons for Eu and Ts respectively. **j,** Representative reconstruction of biocytin filled PNs from Eu and Ts mice. Gray: somatodendritic region (including apical and basal dendrites), red: axon. **k-l,** same as in h-i, but for PNs ($F_{(1, 25)}$=2.487, p=0.1273 2-way ANOVA for apical dendrites; $F_{(1, 25)}$= 0.3521, p=0.5583 2-way ANOVA for basal dendrites). **e,f,** n=14 and 13 neurons for Eu and Ts respectively. **b,c,f,i,l,** Boxplots represent median, percentiles 25 and 75 and whiskers are percentiles 5 and 95. Points represent values from individual synapses (b,c), mice (f), neurons (i,l). *: $p < 0.05$; **: $p < 0.01$

Notably, in Ts mice, action potential width was 1.7-fold wider and input resistance was 1.9-fold of that observed in Eu mice (Figure 3h,i). Conversely, action potential threshold and amplitude were not affected (Supplementary Figure 5, Table 12). Density of PV-INs in mPFC was similar in the two genotypes (Figure 3j). Altogether, these results indicate that, contrary to dendritic inhibition, the synaptic efficiency of the perisomatic feedback loop mediated by PV-INs was normal in Ts mice. Yet, PV-INs of Ts mice lost their characteristic electrophysiological fast-spiking signature, and their excitability was dramatically increased, thus suggesting that the recruitment of PV-INs was facilitated likely producing early ectopic bouts of activity.

In sum, here we report direct evidence for over-inhibition of mPFC circuits in a mouse model of DS, accounting for reduced PN spiking activity and increased tuning of PN action potentials to network oscillations measured *in vivo*. Over-inhibition is due to highly specific synaptic and intrinsic alterations of dendritic and somatic inhibitory circuits, respectively. In this context, it is likely that facilitated recruitment of PV cells fosters neuronal synchrony, as shown in DS subjects[26]. On the other hand, the enhanced MC-PN synaptic loop will likely produce profound alterations of PN dendritic excitability, thus providing a mechanism for impaired synaptic plasticity in Ts mice. This will likely underlie

dysfunctional learning and working memory in DS. In principle, specific alterations in distinct GABAergic circuits found in DS mice could underlie different aspects of cognitive deficits of individuals with DS. Future experiments will be required to reveal whether other GABAergic circuits are affected, and pinpoint the exact mechanisms underlying circuit-specific alterations in DS.

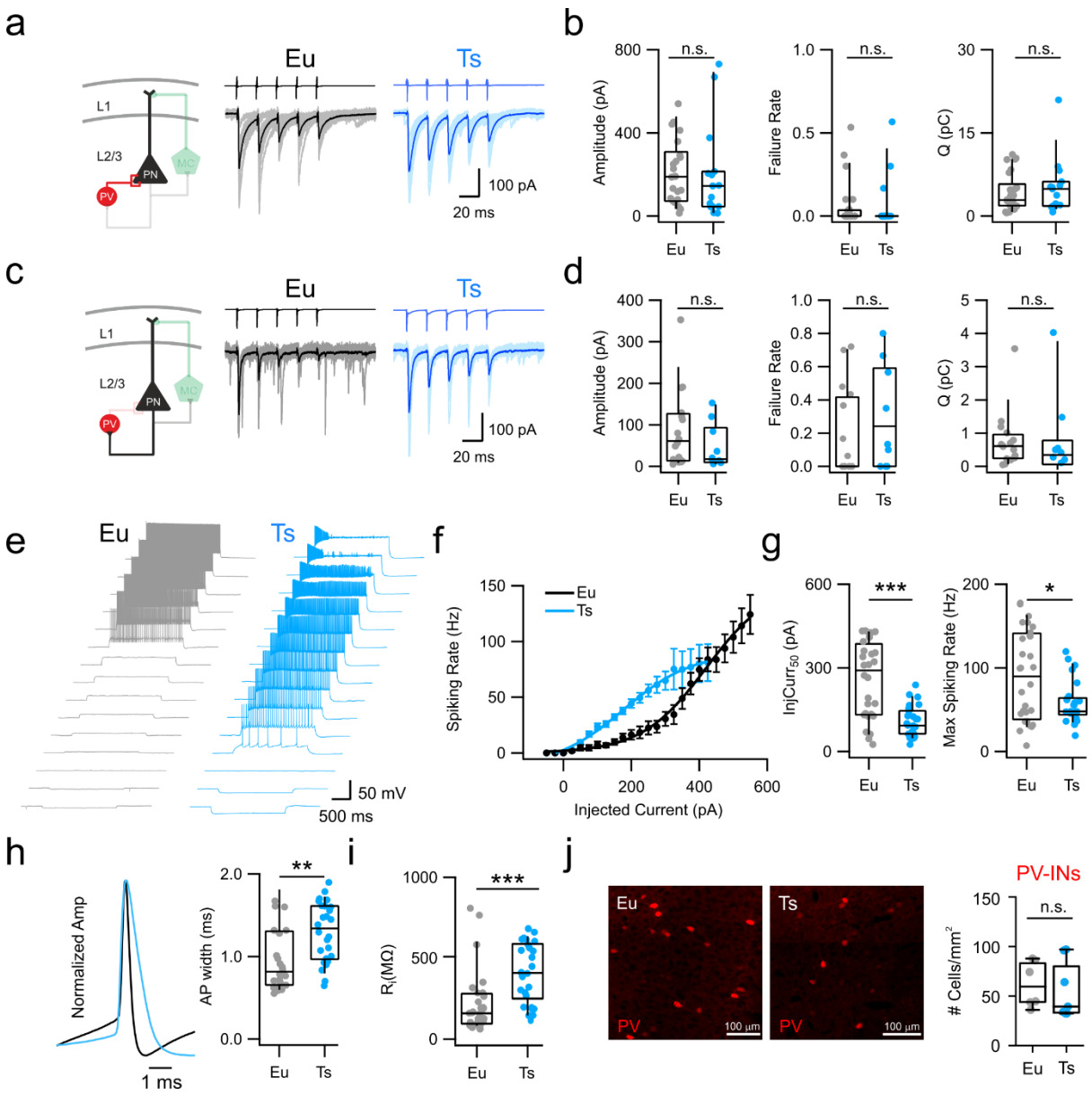

Figure 3: Altered excitability of perisomatic inhibitory PV-INs in Ts mice.

a, Left: scheme of the PV-PN perisomatic inhibitory circuit assessed using dual whole-cell patch-clamp recordings. Right: representative voltage-clamp traces corresponding to uIPSCs evoked upon application of 5 action currents (50 Hz) to the presynaptic PV-IN. Eu: individual (gray) and average (black); Ts: individual (light blue) and average (blue) traces are superimposed. **b,** Population data of uIPSC amplitude (p=0.4901, Mann-Withney U-test), failure rate (p=0.7185, Mann-Withney U-test) and total charge transferred during the 5 APs train (Q, p=0.579, Mann-Withney U-test, n=26 and 15 pairs for Eu and Ts correspondingly). **c-d,** Same as in a-b,

but for glutamatergic uEPSCs triggered in the presynaptic PN and recorded in the postsynaptic PV IN in both genotypes (Amplitude: p=0.233, Mann-Withney U-test; Failure Rate: p=0.214, Mann-Withney U-test; Q: p=0. 3711, Mann-Withney U-test; n=15 and 9 pairs for Eu and Ts correspondingly). **e,** Representative voltage traces in response to current steps of increased amplitudes applied to to PV-INs from Eu (gray) and Ts (blue). **f,** Spiking rate as function of injected current Eu (black) and Ts (blue) mice (Genotype factor $F_{(1, 1040)}$=53.90, P<0.0001, two-way ANOVA; n=28 and 26 cells for Eu and Ts correspondingly). **g,** Left: Population data of the injected current intensity required to reach 50% of maximal spiking rate estimated for each cell in Eu and Ts mice (p=4.55e^{-6}, Mann-Withney U-test). Right: Maximal spiking rate reached upon current injection in the same cells as **g** (p=0.04, Mann-Withney U-test, n=28 and 26 cells for Eu and Ts correspondingly). **h,** Left: representative action-potential traces, scaled to the peak, from Eu (black) and Ts (blue) mice. Right: population data of AP width in the two genotypes. **i,** Population data of input resistance measured in Eu and Ts PV-INs. **j,** Quantification of PV-INs somas in the mPFC of Eu and Ts mice. Left: Epifluorescence images of immunolabeled Parvalbumin in Ts::PV coronal slices. Right: density of PV-INs Eu and Ts (n=6 and 7 mice for Eu and Ts respectively; p=0.2602, Mann-Withney test). *: p < 0.05; **: p < 0.01

References

1. Antonarakis, S. E. Down syndrome and the complexity of genome dosage imbalance. *Nature Reviews Genetics* **18**, 147–163 (2017).
2. Lee, N. R. *et al.* Everyday executive functions in Down syndrome from early childhood to young adulthood: evidence for both unique and shared characteristics compared to youth with sex chromosome trisomy (XXX and XXY). *Front. Behav. Neurosci.* **9**, 264 (2015).
3. Herault, Y. *et al.* Rodent models in Down syndrome research: impact and future opportunities. *Dis. Model. Mech.* **10**, 1165–1186 (2017).
4. Olmos-Serrano, J. L., Tyler, W. A., Cabral, H. J. & Haydar, T. F. Longitudinal measures of cognition in the Ts65Dn mouse: Refining windows and defining modalities for therapeutic intervention in Down syndrome. *Exp. Neurol.* **279**, 40–56 (2016).
5. Zorrilla de San Martin, J., Delabar, J. M., Bacci, A. & Potier, M. C. GABAergic over-inhibition, a promising hypothesis for cognitive deficits in Down syndrome. *Free Radic. Biol. Med.* **114**, 33–39 (2018).
6. Fernandez, F. *et al.* Pharmacotherapy for cognitive impairment in a mouse model of Down syndrome. *Nat. Neurosci.* **10**, 411–413 (2007).
7. Tremblay, R., Lee, S. & Rudy, B. GABAergic Interneurons in the Neocortex: From Cellular Properties to Circuits. *Neuron* **91**, 260–292 (2016).
8. Reeves, R. H. *et al.* A mouse model for Down syndrome exhibits learning and behaviour deficits. *Nat. Genet.* **10**, 196–201 (1995).
9. Ruiz-Mejias, M., Ciria-Suarez, L., Mattia, M. & Sanchez-Vives, M. V. Slow and fast rhythms generated in the cerebral cortex of the anesthetized mouse. *J. Neurophysiol.* **106**, 2910–2921 (2011).

10. Veit, J., Hakim, R., Jadi, M. P., Sejnowski, T. J. & Adesnik, H. Cortical gamma band synchronization through somatostatin interneurons. *Nat. Neurosci.* **20**, 951–959 (2017).

11. Perrenoud, Q., Pennartz, C. M. A. & Gentet, L. J. Membrane Potential Dynamics of Spontaneous and Visually Evoked Gamma Activity in V1 of Awake Mice. *PLoS Biol.* **14**, e1002383 (2016).

12. Cardin, J. A. *et al.* Driving fast-spiking cells induces gamma rhythm and controls sensory responses. *Nature* **459**, 663–667 (2009).

13. Sohal, V. S., Zhang, F., Yizhar, O. & Deisseroth, K. Parvalbumin neurons and gamma rhythms enhance cortical circuit performance. *Nature* **459**, 698–702 (2009).

14. Cho, K. K. A. *et al.* Gamma rhythms link prefrontal interneuron dysfunction with cognitive inflexibility in dlx5/6+/-mice. *Neuron* **85**, 1332–1343 (2015).

15. Abbas, A. I. *et al.* Somatostatin Interneurons Facilitate Hippocampal-Prefrontal Synchrony and Prefrontal Spatial Encoding. *Neuron* **100**, 926-939.e3 (2018).

16. Clem, R. L. & Cummings, K. A. Prefrontal somatostatin interneurons encode fear memory. *Nat. Neurosci.* **23**, p61, 14 p. (2020).

17. Ali, A. B. & Thomson, A. M. Synaptic α5 subunit-containing GABAA receptors mediate ipsps elicited by dendrite-preferring cells in rat neocortex. *Cereb. Cortex* **18**, 1260–1271 (2008).

18. Schulz, J. M., Knoflach, F., Hernandez, M.-C. & Bischofberger, J. Dendrite-targeting interneurons control synaptic NMDA-receptor activation via nonlinear α5-GABAA receptors. *Nat. Commun.* **9**, 3576 (2018).

19. Schulz, J. M., Knoflach, F., Hernandez, M. & Bischofberger, J. Enhanced Dendritic Inhibition and Impaired NMDAR Activation in a Mouse Model of Down Syndrome. *J. Neurosci.* **39**, 5210–5221 (2019).

20. Martínez-Cué, C. *et al.* Reducing GABAA 5 Receptor-Mediated Inhibition Rescues Functional and Neuromorphological Deficits in a Mouse Model of Down Syndrome. *J. Neurosci.* **33**, 3953–3966 (2013).

21. Duchon, A. *et al.* Long-lasting correction of in vivo LTP and cognitive deficits of mice modelling Down syndrome with an α5-selective GABAA inverse agonist. *Br. J. Pharmacol.* 1–13 (2019). doi:10.1111/bph.14903

22. Braudeau, J. *et al.* Specific targeting of the GABA-A receptor {alpha}5 subtype by a selective inverse agonist restores cognitive deficits in Down syndrome mice. *J. Psychopharmacol.* **25**, 1030–1042 (2011).

23. Ma, Y. Distinct Subtypes of Somatostatin-Containing Neocortical Interneurons Revealed in Transgenic Mice. *J. Neurosci.* **26**, 5069–5082 (2006).

24. Dawson, G. R. *et al.* An Inverse Agonist Selective for ␣ 5 Subunit-Containing GABA. *J.*

Pharmacol. Exp. Ther. **316**, 1335–1345 (2006).

25. Kaiser, T., Ting, J. T., Monteiro, P. & Feng, G. Transgenic labeling of parvalbumin-expressing neurons with tdTomato. *Neuroscience* **321**, 236–245 (2016).

26. Anderson, J. S. *et al.* Abnormal brain synchrony in Down Syndrome. *NeuroImage Clin.* **2**, 703–715 (2013).

27. Zucca, S. *et al.* An inhibitory gate for state transition in cortex. *Elife* **6**, 1–31 (2017).

Methods

Experimental procedures followed national and European (2010/63/EU) guidelines, and have been approved by the authors' institutional review boards and national authorities. All efforts were made
305 to minimize suffering and reduce the number of animals. Experiments were performed on >4 week old and 18- to 25-day-old mice for *in vivo* and *ex vivo* recordings, respectively. We used *B6EiC3Sn a/A-Ts(17 ^{16})65Dn/J* (also known as Ts65Dn) mice (The Jackson Laboratory, Bar Harbor, Maine; stock #: 001924). For *ex vivo* slice experiments to label SST-positive MCs, Ts65Dn mice were crossed with *Tg(Gad1-EGFP)98Agmo/J*, also known as GAD67-GFP X98 or GFP-X98 (Jackson Laboratory). To label
310 PV-INs, Ts65Dn mice were crossed with *C57BL/6-Tg(Pvalb-tdTomato)15Gfng/J* (*Pvalb-tdTomato*, Jackson Laboratory). Mice used in this study were of both sexes.

In vivo LFP and juxtacellular recordings

Ts or Eu mice were anesthetized with 15% urethane (1.8 g/kg in physiological solution) and placed on a stereotaxic apparatus. The body temperature was constantly monitored and kept at 37 °C with a
315 heating blanket. To ensure a deep and constant level of anesthesia, vibrissae movement, eyelid reflex, response to tail, and toe pinching were visually controlled before and during the surgery. A local lidocaine injection was performed over the cranial area of interest and, after a few minutes, a longitudinal incision was performed to expose the skull. Two small cranial windows (around 1 mm diameter) were opened at at 2.5 mm from bregma and ± 1 mm lateral to sagittal sinus (corresponding
320 to the frontal lobe) carefully avoiding any damage to the main vessels while keeping the surface of the brain moist with the normal HEPES-buffered artificial cerebrospinal fluid. The dura was carefully removed using a metal needle. Glass pipettes used to record LFP had 1-2 MΩ resistance while those used for juxtacellular patch-clamp recordings typically had 5-7MΩ resistance. LFP and patch electrodes were pulled from borosilicate glass capillaries. Signals were amplified with a Multiclamp
325 700B patch-clamp amplifier (Molecular Devices), sampled at 20 KHz and filtered online at 10 KHz.

Signals were digitized with a Digidata 1440A and acquired, using the pClamp 10 software package (Molecular Devices).

Preparation of acute slices for electrophysiology

In order to record intrinsic and synaptic properties of L2/3 neurons of mPFC, we prepared acute
330 cortical slices from the described mouse lines. For these experiments, we used slices cut in the coronal plane (300-350 µm thick). Animals were deeply anesthetized with saturating isofluorane (Vetflurane, Virbac) and immediately decapitated. The brain was then quickly removed (for groups of mice aged <P20, this procedure started right after deep anesthesia) and immersed in the cutting choline-based solution, containing the following (in mM): 126 choline chloride, 16 glucose, 26 $NaHCO_3$, 2.5 KCl,
335 1.25 NaH_2PO_4, 7 $MgSO_4$, 0.5 $CaCl_2$, cooled to 4°C and equilibrated with a 95-5% O_2-CO_2 gas mixture. Slices were cut with a vibratome (Leica VT1200S) in cutting solution and then incubated in oxygenated artificial cerebrospinal fluid (aCSF) composed of (in mM): 126 NaCl, 20 glucose, 26 $NaHCO_3$, 2.5 KCl, 1.25 NaH_2PO_4, 1 $MgSO_4$, 2 $CaCl_2$ (pH 7.35, 310-320mOsm/L), initially at 34°C for 30 min, and subsequently at room temperature, before being transferred to the recording chamber where
340 recordings were obtained at 30–32°C.

Slice electrophysiology

Whole-cell patch-clamp recordings were performed in L2/3 of the medial prefrontal cortex (mPFC) neurons. Inhibitory PV-expressing interneurons, labeled with TdTomato in Ts65Dn mice crossed with *Pvalb-tdTomato* mice and Martinotti cells, labeled with GFP in Ts65Dn crossed with GFP-X98 mice,
345 were identified using LED illumination (OptoLED, Cairn Research, Faversham, UK). Excitatory pyramidal neurons (PNs) were visually identified using infrared video microscopy, as cells lacking expression of fluorescent proteins and with somatas exhibiting the classical pyramidal shape. Accordingly, when depolarized with DC current pulses PNs exhibited a typical firing pattern of regular-spiking cells. We used different intracellular solutions depending on the type of experiment and the
350 nature of the responses we wanted to assess. To study passive properties, intrinsic excitability, AP

waveform and glutamatergic spontaneous transmission, electrodes were filled with an intracellular solution containing (in mM): 127 K-gluconate, 6 KCl, 10 Hepes, 1 EGTA, 2 MgCl2, 4 Mg-ATP, 0.3 Na-GTP; pH adjusted to 7.3 with KOH; 290–300 mOsm. The estimated reversal potential for chloride (E_{Cl}) was approximately −69 mV based on the Nernst equation. To measure GABAergic currents elicited by
355 perisomatic-targeting interneurons, PNs were patched using an intracellular solution containing (in mM): 65 K-gluconate, 70 KCl, 10 Hepes, 1 EGTA, 2 MgCl2, 4 Mg-ATP, 0.3 Na-GTP; pH adjusted to 7.3 with KOH; 290–300 mOsm (the estimated ECl was approximately −16 mV based on the Nernst equation). For distal dendritic uIPSCs, we used a cesium-based solution containing (in mM): 145 CsCl, 10 Hepes, 1 EGTA, 0.1 CaCl2, 2 MgCl2, 4.6 Mg-ATP, 0.4 Na-GTP, 5 QX314-Cl; pH adjusted to 7.3 with
360 CsOH; 290–300 mOsm. Under these recording conditions, activation of $GABA_A$ receptors resulted in inward currents at a holding potential (Vh) of −70 mV. Voltage values were not corrected for liquid junction potential. Patch electrodes were pulled from borosilicate glass capillaries and had a typical tip resistance of 2–3 MΩ. Signals were amplified with a Multiclamp 700B patch-clamp amplifier (Molecular Devices), sampled at 20–50 KHz and filtered at 4 KHz (for voltage-clamp experiments) and
365 10 KHz (for current-clamp experiments). Signals were digitized with a Digidata 1440A and acquired, using the pClamp 10 software package (Molecular Devices).

For paired recordings, unitary synaptic responses were elicited in voltage-clamp mode by brief somatic depolarizing steps (-70 to 0 mV, 1-2 ms) evoking action currents in presynaptic cells. Neurons were held at −70 mV and a train of 5 presynaptic spikes at 50 Hz was applied.

370 ***Immunohistochemistry***

Parvalbumin, SST and GFP staining were performed on 20-50 µm-thick slices. Briefly, mice were perfused with 0.9% NaCl solution containing Heparin and 4% paraformaldehyde (PFA). Brains were cryo-protected by placing them overnight in 30% sucrose solution and then frozen in Isopentane at a temperature <-50°C. Brains were sliced with a freezing microtome (ThermoFisher HM450).
375 Permeabilization in a blocking solution of PBT with 0.3% Triton and 10% Normal Goat Serum was done

at room temperature for 2 hr. Slices were then incubated overnight (4°C) in the same blocking solution containing the primary rabbit anti-PV antibody (1:1000; Thermo Scientific) and mouse anti-SST antibody (1:250; Santa Cruz Biotechnologies). Slices were then rinsed three times in PBS (10 min each) at room temperature and incubated with goat anti-rabbit and a goat anti-mouse antibody (1:500;
380 Jackson IR) coupled to Alexa-488 or 633 for 3.5 hr at room temperature. Slices were then rinsed three times in PBS (10 min each) at room temperature and coverslipped in mounting medium (Fluoromount, Sigma Aldrich **F4680**). Immunofluorescence was then observed with a slide scanner (Zeiss, Axio Scan.Z1).

Morphological reconstruction

385 Biocytin Fills: To reliably reconstruct the fine axonal branches of cortical neurons, dedicated experiments were performed following the classical avidin-biotin-peroxidase method. Biocytin (Sigma) was added to the intracellular solution at a high concentration (5-10mg/ml), which required extensive sonication. At the end of recordings, the patch pipette was removed carefully until obtaining an inside out patch. The slice was then left in the recording chamber for at least further 5-
390 10 min to allow further diffusion. Slices were then fixed with 4% paraformaldehyde in phosphate buffer saline (PBS, Sigma) for at least 48 h. Following fixation, slices were incubated with the avidin-biotin complex (Vector Labs) and a high concentration of detergent (Triton-X100, 5%) for at least two days before staining with 3,3'Diaminobenzidine (DAB, AbCam). Cells were then reconstructed and cortical layers delimited using Neurolucida 7 (MBF Bioscience) and the most up to date mouse atlas
395 (Allen Institute).

Data analysis

Electrophysiological and statistical analysis was performed using built-in and custom-written routines made for Igor Pro (WaveMetrics, Lake Oswego, OR, USA), MATLAB R2017b 9.3.0.713579 Natick, Massachusetts: The MathWorks Inc.; Origin (Pro) 2016 OriginLab Corporation, Northampton, MA,

USA; Prism version 7.00 for Windows, GraphPad Software, La Jolla California USA; and Python Software Foundation. Python Language Reference, version 3.6, available at http://www.python.org.

Analysis of in vivo recordings:

Traces obtained from juxtacellular recording were high pass filtered (cutoff: 5 Hz) and spikes were detected based on threshold=1.5 mV. Spike rate was estimated as the total number of spikes detected divided by the total duration of the recording. The peak time (t_{peak}) corresponding to each detected action potential was used to select the segment of LFP between: [t_{peak}-100 ms to t_{peak}+100 ms]. The instantaneous phase was estimated using Hilbert transform on decimated LFP and subsequently used to estimate phase locking. For LFP analysis, extracellular potentials were down-sampled (1 kHz) and low- pass filtered (cutoff frequency, 100 Hz). Power spectra were generated using a Hann window (window length: 4096 points, 50% overlap).

Phase locking was determined using pairwise phase consistency (PPC) estimation, defined as:

$$PPC_f = \frac{2 * \left(\sum_{i=1}^{N-1} \sum_{j=i+1}^{N} \left(cos(\theta_i).cos(\theta_j) + sin(\theta_i).sin(\theta_j)\right)\right)}{N.(N-1)}$$

Where N is the total number of action potentials and θ_i is the phase of the ith spike and θ_j the jth.

UP and DOWN states detection

Cortical states were detected as described elsewhere[27]. Briefly, filtered and decimated LFP was used to calculate UP and DOWN state likelihood decision (or evidence) variable (S_{comb}) based on low frequency (<4Hz) oscillation phase and high frequencies (20–100Hz) composition of the LFP. To determine the thresholds to detect different cortical states (UP, Intermediate, DOWN) states, the distribution of the combined evidence variable, S_{comb}, was fitted by a mixture of three Gaussians, each representing their corresponding cortical state, UP (highest level of the signal), Intermediate (Intermediate level) and DOWN (lowest level of the signal). Periods of the combined signal, S_{comb}, that were above the UP threshold, $\mu_{UP-LFP} - 3 * \sigma_{UP-LFP}$, were considered the periods of UP states.

Similarly, the periods below the DOWN threshold, $\mu_{DOWN-LFP} - 3 * \sigma_{DOWN-LFP}$, were considered the periods of DOWN states (means and variances of the Gaussians are represented as μ_{UP}, μ_{DOWN}, and σ_{UP}, σ_{DOWN} for the up and down cortical states, respectively). Periods of UP and DOWN states were refined further by putting constraints on the interval between two states and duration of a state. Minimum interval between two states and duration of a state were set 50 and 70 ms, respectively.

Analysis of slices electrophysiological recordings

Input resistance (R_i) was estimated as the slope of the current to voltage relationship obtained with upon the injection of -25, 0 and 25 pA to a cell kept at resting potential. Membrane time constant was measured estimated fitting the time course of V_{memb} after the injection of a 2s, -25 pA current step.

We used protocols of increasing steps of current injection (-50 to 500 pA in steps of 25 or 50 pA and 2 seconds duration). Action potentials were detected using a threshold based routine. Threshold was set at 0 mV. Firing dynamics was evaluated fitting F-I curves from individual cells to a sigmoidal function:

$$f(x) = base + \left\{max\left[1 + e^{\frac{(\mathrm{InjCurr}_{50} - x)}{rate}}\right]\right\}$$

Where *base*: minimal spiking rate, *max*: maximal spiking rate achieved, $\mathrm{InjCurr}_{50}$: current injected necessary to reach 50% of *max,* and *rate*: the gain. The first action potential evoked was taken to measure amplitude, width and threshold. Threshold was considered as the potential at which dV/dt reached 10 mV/ms; amplitude was the difference between peak amplitude and threshold and half-width was the time interval between rise and decay phase measured at 50% of amplitude.

Action potential threshold was defined as the membrane potential value (V_m) at which dV/dt become bigger than 10 mV/ms. Action potential amplitude is: $Amp = Amp_{peak} - threshold$ where Amp_{peak} is the AP peak potential. Action potential width was measured at 50% of amplitude.

Statistical analysis:

Normal distribution of samples was systematically assessed (Shapiro-Wilkinson normality test). Normal distributed samples were statistically compared using two-tailed Student's *t* test unless otherwise stated. When data distribution was not normal we used two-tailed Mann Whitney U-test. Compiled data are reported and presented as whisker box plots (the upper and lower whiskers
450 representing the 90th and 10th percentiles, respectively, and the upper and lower boxes representing the 75th and 25th percentiles, respectively, and the horizontal line representing the median or the mean ± s.e.m., with single data points plotted. Differences were considered significant if $p<0.05$ (*$p<0.05$, **$p<0.01$, ***$p<0.001$).

Supplementary information

Alterations of specific inhibitory circuits of the prefrontal cortex underlie abnormal network activity in a mouse model of Down syndrome

Javier Zorrilla de San Martin[1*], Cristina Donato[1,2], Jérémy Peixoto[1], Andrea Aguirre[1], Vikash Choudhary[1], Angela Michela De Stasi[1], Joana Lourenço[1], Marie-Claude Potier[1*] and Alberto Bacci[1*]

Supplementary figures

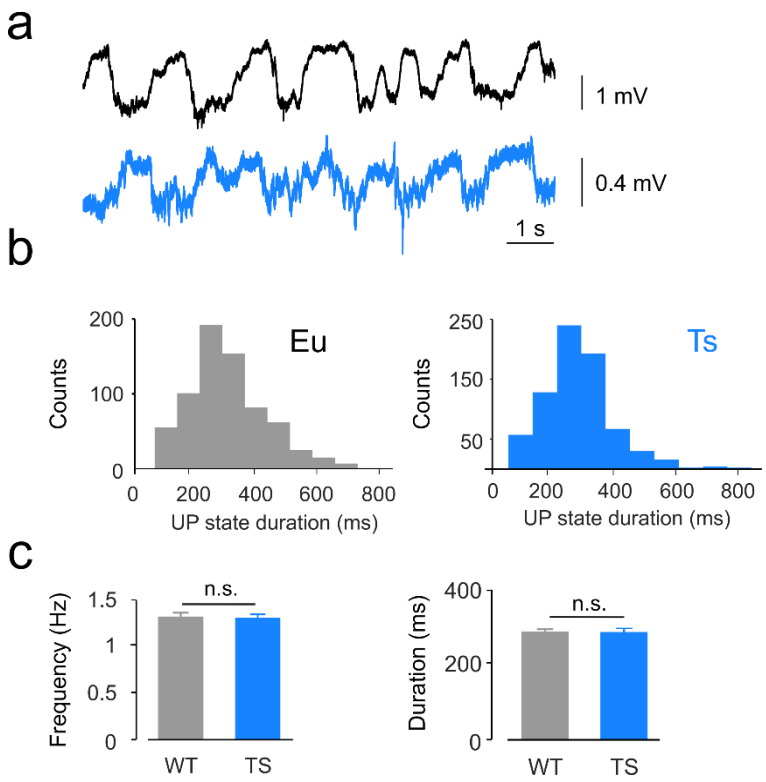

Supplementary figure 1: Characterization of slow wave oscillatory activity of LFP in anesthetized Eu and Ts mice.

a, Representative LFP traces of anesthetized Eu (black, top) and Ts (bottom, blue) mice. **b,** Histograms of UP states duration from the examples shown in **a**, Eu (gray bars) and Ts (blue bars) examples. **c,** Average frequency, population data (left panel; Eu: 1.32 ± 0.02 Hz, Ts: 1.33 ± 0.02 Hz; Student's T test, p= 0.86952) and average duration (right panel; Eu: 305.0 ± 3.3 ms, Ts: 310.9 ± 4.1 ms; Student's T test, p=0.6352) of UP state did not significantly differed between genotypes (n=6 and 7 mice correspondingly).

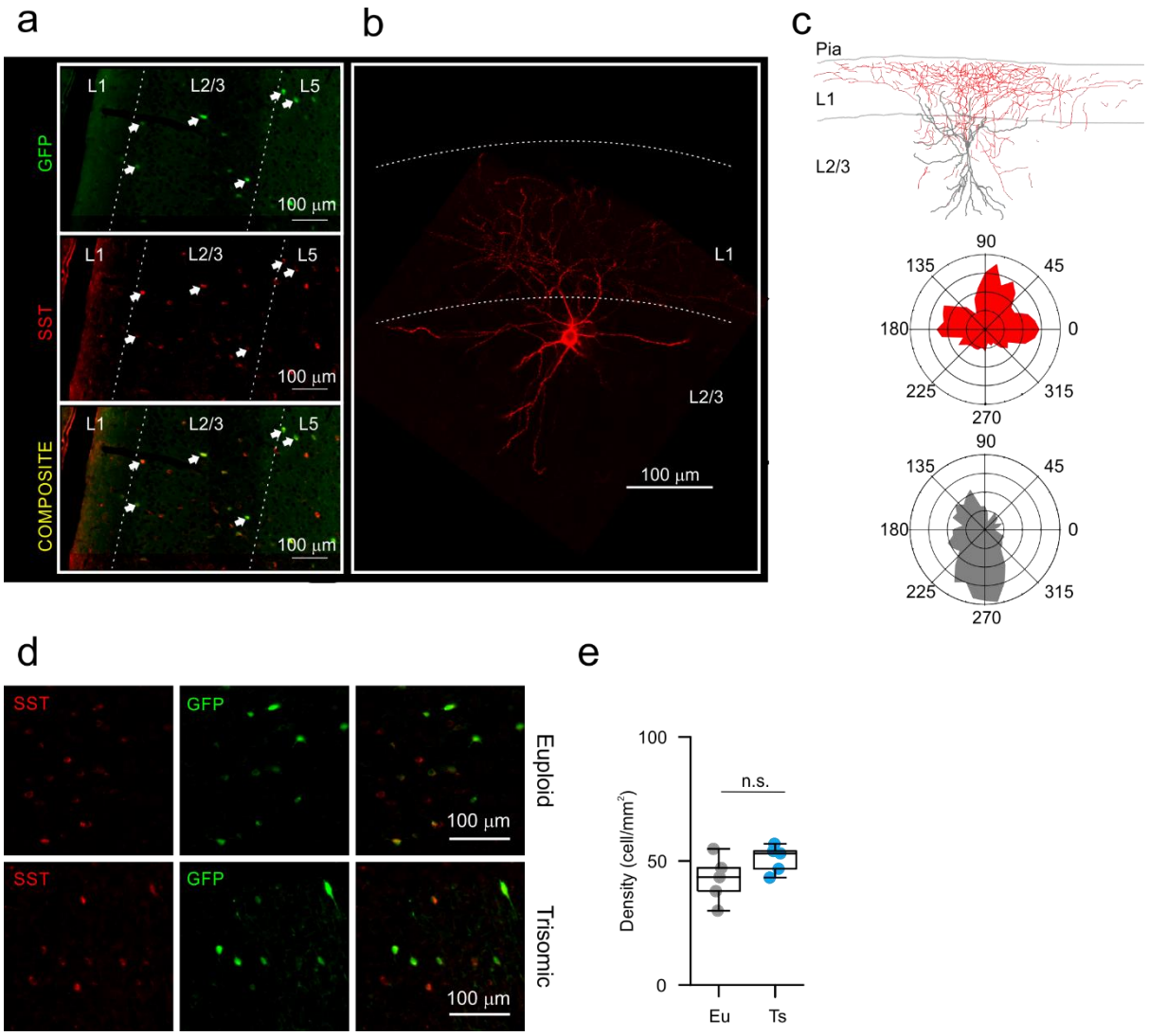

Supplementary figure 2: GFP positive interneurons in the prefrontal cortex of Ts::X98 mice are Martinotti cells.

a, Immunostaining of GFP (green) and SST (red) in the mPFC. Note the co-localization of both markers. Arrows point to GFP and SST. **b,** Biocytin-filled GFP-positive interneuron revealed with Texas red coupled to Streptavidin. Note the wide extension of the axonal plexus of Ts::X98 GFP-positive neurons in layer 1, typical of Martinotti cells. **c,** Top: Reconstructed morphology of the biocytin-filled cell of b and the polar histograms of its axonal (blue) and dendritic (pink) densities. **d**, GFP and SST immunostaining in both genotypes. **e**, Quantification of SST-positive cells density in mPFC L2/3 from Eu and Ts Ts::X98 mice.

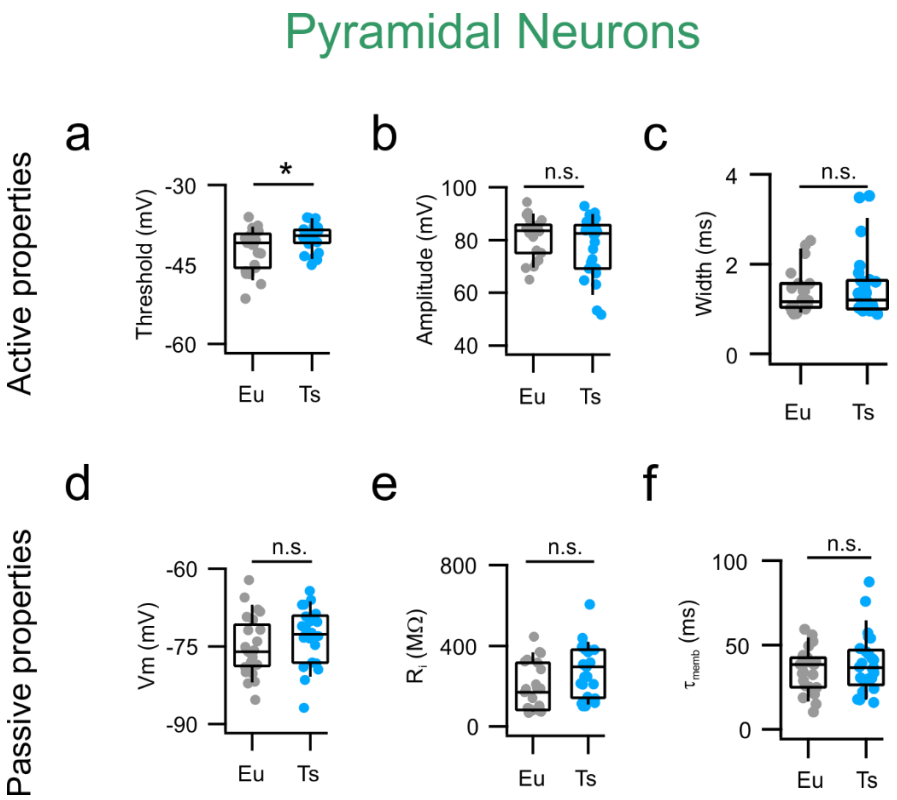

Supplementary figure 3: Single action potential and passive properties are normal Ts mPFC PNs.

a, AP thresholds estimated as the voltage at which the derivative of Vm as function of time (dV/dt) reaches the limit of 10 mV/ms. Eu: -41 mV, -45-39 mV (n=23 cells) and Ts: -40, -41-39 mV mV (n=25 cells; Mann-Whitney U-test, p = 0.0453). **b,** AP amplitude measured as the difference between Vm at threshold and Vm at peak Eu: 84, 75-86 mV (n=23 cells) and Ts: 82, 69-85 mV (n=25 cells; Mann-Whitney U-test, p = 0.37486). **c,** AP width measured as the time interval between the up stroke and the repolarization phase at half amplitude was not significantly different between genotypes. Eu: 1.2, 1-1.6 ms (n=23 cells) and Ts: 1.2, 1-1.6 ms (n=25 cells; p = 0.74125, Mann-Whitney U-test). **d,** Resting membrane potential was also not significantly different between genotypes. Eu: -76, -79-72 mV (n=23 cells) and Ts: -73, -78-69 mV (n=25 cells; p = 0.74125, Mann-Whitney U-test). **e,** Input resistance, Eu: 255, 139-378 MΩ (n=23 cells), Ts: 178, 86-316 MΩ (n=25 cells, p=0.05918, Mann-Whitney U-test). **f,** Decay tau of the membrane Eu: 37, 28-48 (n=23 cells), Ts: 40, 27-47 (n=25 cells, p=0.90665, Mann-Whitney U-test). Boxplots: represent median, percentiles 25 and 75 and whiskers are percentiles 5 and 95. Individual points represent average values from individual cells.

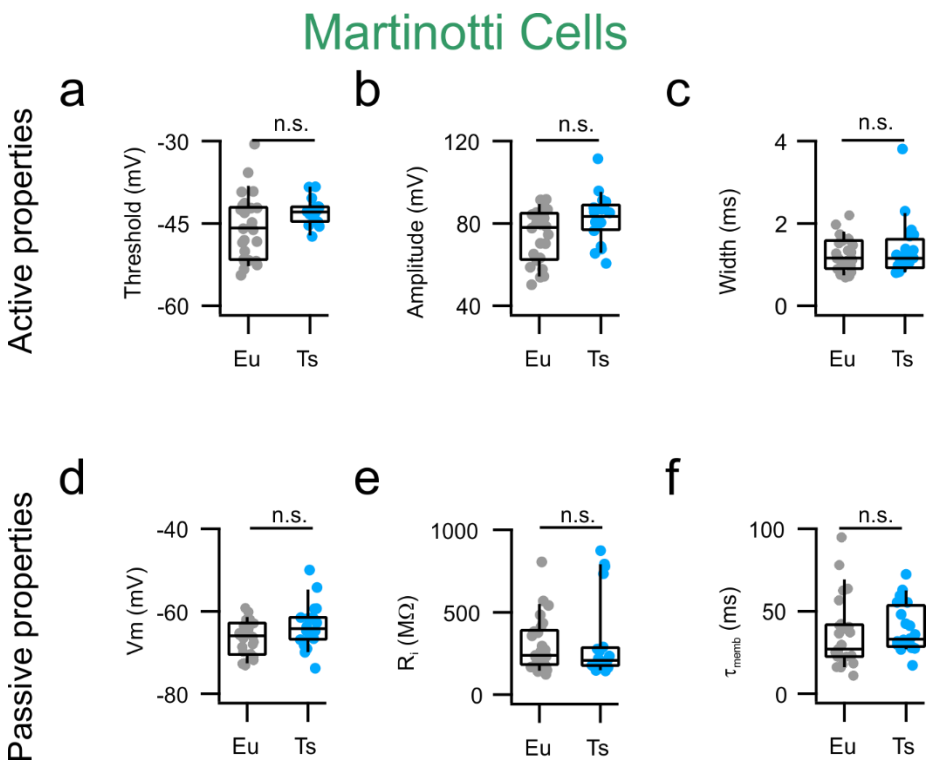

Supplementary figure 4: Active and passive properties are normal in mPFC MCs from Ts65Dn mice.

a, AP thresholds estimated as the voltage at which the derivative of Vm as function of time (dV/dt) reaches the limit of 10 mV/ms. Eu: -46, -52-42 (n=23 cells); Ts: -43, -45-42 (n=25 cells, p=0.09877, Mann-Whitney U-test). **b,** AP amplitude measured as the difference between Vm at threshold and Vm at peak Eu: 79, 63-85 mV (n=26 cells), Ts: 82, 69-85 mV (n=20, p=0.07267, Mann-Whitney U-test). **c,** AP width measured as the time interval between the up stroke and the repolarization phase at half amplitude was not significantly different between genotypes. Eu: 1.2, 0.9-1.6 ms (n=26 cells), Ts: 1.2, 0.9-1.6 ms (n=20 cells, p=0.8680, Mann-Whitney U-test). **d,** Resting membrane potential. Eu: -66, -70-63 (n=26 cells), Ts: -64, -67-62 (n=20 cells, p=0.0566, Mann-Whitney U-test). **e,** Input resistance, Eu: 238, 183-382 MΩ (n=26 cells), Ts: 207, 176-282 MΩ (n=20 cells, p=0.57205, Mann-Whitney U-test). **f,** Decay tau of the membrane Eu: 27, 22-41 (n=26 cells), Ts: 33, 29-52 (n=20 cells, p=0.14067, Mann-Whitney U-test). Boxplots: represent median, percentiles 25 and 75 and whiskers are percentiles 5 and 95. Individual points represent average values from each recorded synaptic connection.

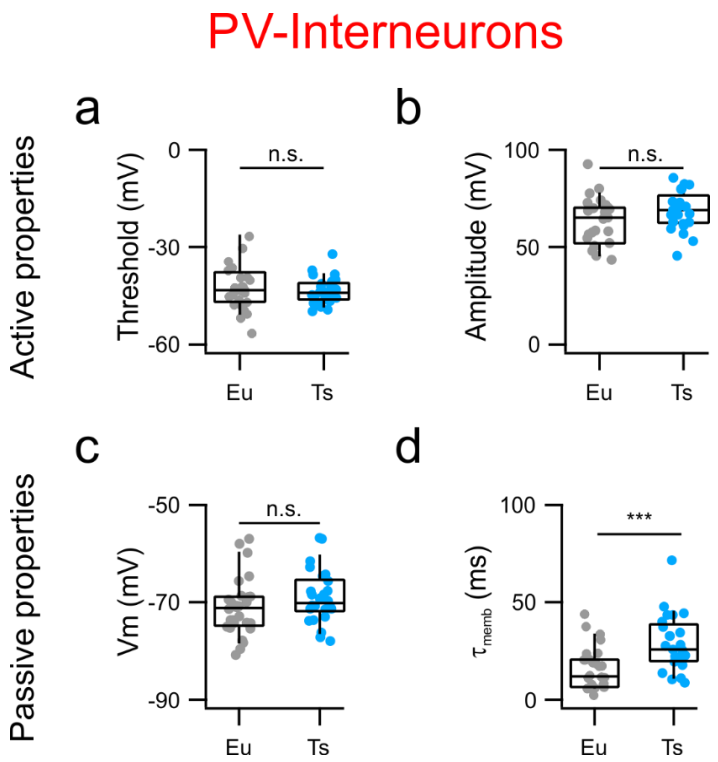

Supplementary figure 5: Specific alteration of mPFC PV-INs electrical properties in Ts65Dn mice.

a, AP thresholds estimated as the voltage at which the derivative of Vm as function of time (dV/dt) reaches the limit of 10 mV/ms. Eu: -43 mV -47--39 (n=26 cells), Ts: -44 mV -46--41 (n=26 cells; p=0.0988 Student's T test). **b,** AP amplitude measured as the difference between Vm at threshold and Vm at peak Eu: 79, 63-85 mV (n=26 cells), Ts: 69, 63-73 mV (n=26, p=0.8680, Mann-Whitney U-test). **c,** Resting membrane potential. Eu: -71, -75--69 (n=26 cells), Ts: -69, -71--66 (n=26 cells, p=0.0566, Student's T test). **d,** Decay tau of the membrane Eu: 12, 7-21 ms (n=26 cells), Ts: 26, 20-37 ms (n=25 cells, p=0.14067, Mann-Whitney U-test). Boxplots: represent median, percentiles 25 and 75 and whiskers are percentiles 5 and 95. Individual points represent average values from each recorded synaptic connection.

Supplementary Tables

Ts65Dn in vivo activity

Supplementary table 1: LFP and single cell spiking recorded in vivo.

		Euploid					Ts65Dn						
		median	**Q1**	**Q3**	**N cells**	**N mice**	**median**	**Q1**	**Q3**	**N cells**	**N mice**	**test**	**p value**
	Spiking Rate (Hz)	0.81	0.56	1.24	28	6	0.42	0.22	0.92	23	5	MW-test	0.0348
stLFP	peak-to-peak Amp (µV)	7.3	6.0	8.6	22	6	13.3	12.3	17.1	11	5	MW-test	0.0011

Median: quantile 50; Q1: quantile 25; Q3: quantile 75; n: number of cells.

Supplementary table 2: Pairwise Phase Consistency (PPC) descriptive statistics and hypothesis tests between genotypes for each frequency band analyzed.

		Euploid					Ts65Dn						
	Freq. band	**median**	**Q1**	**Q3**	**N cells**	**N mice**	**median**	**Q1**	**Q3**	**N cells**	**N mice**	**test**	**p value**
PPC	4-10 Hz	0.0085	0.0053	0.0242	22	6	0.0106	0.0064	0.0164	11	5	MW-test	0.4270
	10-20 Hz	0.0046	0.0011	0.0237	22	6	0.0213	0.0163	0.0379	11	5	MW-test	0.0215
	20-40 Hz	0.0024	-0.0002	0.0085	22	6	0.0066	0.0059	0.0193	11	5	MW-test	0.0418
	40-60 Hz	0.0009	-0.0009	0.0025	22	6	0.0052	0.0019	0.0079	11	5	MW-test	0.0164
	60-80 Hz	-0.0003	-0.0007	0.0004	22	6	0.0001	-0.0005	0.0009	11	5	MW-test	0.2308
	80-100 Hz	-0.0002	-0.0009	0.0013	22	6	-0.0004	-0.0008	0.0002	11	5	MW-test	0.3161

Median: quantile 50; Q1: quantile 25; Q3: quantile 75; n: number of cells. We considered only cells from which we recorded at least 250 action potentials in order to obtain reliable PPC values.

Dendritic inhibition

540 Evaluation of synaptic efficiency in the dendritic inhibitory loop composed by MCs and PNs.

Supplementary table 3: MC to PN synaptic efficiency evaluation.

		Dendritic Inhibition									
		Euploid				Ts65Dn					
		median	Q1	Q3	n	median	Q1	Q3	n	test	p value
MC-PN IPSC	Amplitude (pA)	29.89	20.24	52.98	11	97.09	54.49	135.86	15	MW-test	0.0095
	Failure Rate	0.20	0.11	0.25	11	0.00	0.00	0.13	15	MW-test	0.0201
	Charge (pC)	1.28	0.96	1.84	11	6.86	2.96	8.32	15	MW-test	0.00595
	α5IA % block	41	24.20	57.20	4	57.4	33.10	73.10	6	MW-test	0.2278

Median: quantile 50; Q1: quantile 25; Q3: quantile 75; n: number of cells; IPSC: Inhibitory
545 postsynaptic current.

Supplementary table 4: PN to MC synaptic efficiency evaluation.

		Dendritic Inhibition									
		Euploid				Ts65Dn					
		median	Q1	Q3	n	median	Q1	Q3	n	test	p value
PN-MC EPSC	Amplitude (pA)	5.36	2.13	7.46	7	18.66	11.44	28.21	7	T-test	0.0106
	Failure Rate	0.87	0.81	0.93	7	0.52	0.39	0.71	7	MW-test	0.0126
	Charge (pC)	0.27	0.22	0.31	7	0.87	0.53	1.13	7	MW-test	0.0073

Median: quantile 50; Q1: quantile 25; Q3: quantile 75; n: number of cells; EPSC: Excitatory
550 postsynaptic current.

Supplementary table 5: PNs excitability.

		Euploid				Ts65Dn					
		median	**Q1**	**Q3**	**n**	**median**	**Q1**	**Q3**	**n**	**test**	**p value**
Excitability	InjCurr50 (pA)	21.6	19.5	24.4	12	18.9	15.9	24.6	11	T-test	0.6081
	Max Spiking Rate (Hz)	112.4	91.9	155.0	12	124.5	101.0	178.2	11	T-test	0.4500

Median: quantile 50; Q1: quantile 25; Q3: quantile 75; n: number of cells; InjCurr50: amount of current injected to reach 50% of the maximal spiking rate.

555

Supplementary table 6: MCs excitability.

		Euploid				Ts65Dn					
		median	**Q1**	**Q3**	**n**	**median**	**Q1**	**Q3**	**n**	**test**	**p value**
Excitability	InjCurr50 (pA)	40.9	26.9	50.4	25	48.9	25.4	70.2	20	MW-test	0.6073
	Max Spiking Rate (Hz)	101.8	68.3	124.0	25	86.5	63.2	109.7	20	T-test	0.4436

Median: quantile 50; Q1: quantile 25; Q3: quantile 75; n: number of cells; InjCurr50: amount of current injected to reach 50% of the maximal spiking rate.

560

Supplementary table 7: PNs passive and action potential (AP) properties.

		Euploid				Ts65Dn					
		median	**Q1**	**Q3**	**n**	**median**	**Q1**	**Q3**	**n**	**test**	**p value**
Passive properties	Vrest (mV)	-76	-79	-72	25	-73	-78	-69	22	T-test	0.2473
	Ri (MΩ)	255	139	378	25	178	86	316	22	T-test	0.7185
	Tau memb (ms)	36.5	28.1	47.9	25	39.7	26.8	46.9	22	T-test	0.5790
AP properties	Threshold (mV)	-40.9	-45.6	-39.2	25	-39.6	-40.8	-38.5	22	MW-test	0.0453
	Amplitude (mV)	83.6	75.1	85.8	25	82.5	69.2	85.5	22	MW-test	0.3749
	Width (ms)	1.2	1.0	1.6	25	1.2	1.0	1.6	22	MW-test	0.7413

Median: quantile 50; Q1: quantile 25; Q3: quantile 75; n: number of cells; Vrest: Resting membrane potential; Ri : input resistance.

565

Supplementary table 8: MCs passive and action potential (AP) properties.

		Euploid				Ts65Dn					
		median	**Q1**	**Q3**	**n**	**median**	**Q1**	**Q3**	**n**	**test**	**p value**
Passive properties	Vrest (mV)	-66	-70	-63	26	-64	-67	-62	20	T-test	0.0566
	Ri (MΩ)	238	183	382	26	207	176	282	20	MW-test	0.5721
	Tau memb (ms)	27.0	22.4	41.4	25	33.0	28.7	51.7	20	MW-test	0.1407
AP properties	Threshold (mV)	79.0	63.2	85.1	26	83.4	77.3	88.5	20	MW-test	0.0988
	Amplitude (mV)	-45.8	-51.5	-42.2	26	-42.9	-44.6	-42.0	20	MW-test	0.0727
	Width (ms)	1.2	0.9	1.6	26	1.2	0.9	1.5	20	MW-test	0.8680

Median: quantile 50; Q1: quantile 25; Q3: quantile 75; n: number of cells; Vrest: Resting membrane potential ; Ri : input resistance.

570

Perisomatic inhibition

Evaluation of synaptic efficiency in the perisomatic inhibitory loop composed by PVs and PNs.

575

Supplementary table 9: Direct perisomatic inhibition. PV to PN synaptic efficiency evaluation.

		Perisomatic inhibition									
		Euploid				Ts65Dn					
		median	Q1	Q3	n	median	Q1	Q3	n	test	p value
PV-PN IPSC	Amplitude (pA)	188.43	74.87	289.03	26	144.52	46.10	209.78	15	MW-test	0.49
	Failure Rate	0.00	0.00	0.03	26	0.00	0.00	0.00	15	MW-test	0.7185
	Charge (pC)	2.88	1.92	5.02	26	4.89	1.89	5.85	15	MW-test	0.579

Median: quantile 50; Q1: quantile 25; Q3: quantile 75; n: number of cells; IPSC: Inhibitory postsynaptic current.

580

Supplementary table 10: Recruitment of PV-INs by PNs. PN to PV synaptic efficiency evaluation.

		Perisomatic inhibition									
		Euploid				Ts65Dn					
		median	Q1	Q3	n	median	Q1	Q3	n	test	p value
PN-PV EPSC	Amplitude (pA)	65.66	19.28	124.50	15	20.41	14.10	84.25	9	MW-test	0.23304
	Failure Rate	0.00	0.00	0.27	15	0.13	0.00	0.57	9	MW-test	0.21402
	Charge (pC)	0.62	0.29	0.90	15	0.42	0.20	0.55	9	MW-test	0.3711

Median: quantile 50; Q1: quantile 25; Q3: quantile 75; n: number of cells; EPSC: Excitatory postsynaptic current.

585

Supplementary table 11: PV-INs passive and action potential (AP) properties.

		Euploid				Ts65Dn					
		median	**Q1**	**Q3**	**n**	**median**	**Q1**	**Q3**	**n**	**test**	**p value**
Excitability	InjCurr50 (pA)	310.4	136.3	394.6	26	92.9	63.5	142.7	26	MW-test	0.0003
	Max Spiking Rate (Hz)	99.5	45.2	142.3	26	47.9	45.3	63.3	26	MW-test	0.0001

Median: quantile 50; Q1: quantile 25; Q3: quantile 75; n: number of cells; InjCurr50: amount of current injected to reach 50% of the maximal spiking rate.

590

Supplementary table 12: PV-INs passive and action potential (AP) properties.

		Euploid				Ts65Dn					
		median	**Q1**	**Q3**	**n**	**median**	**Q1**	**Q3**	**n**	**test**	**p value**
Passive properties	Vrest (mV)	-71	-75	-69	28	-70	-71	-66	26	T-test	0.1808
	Ri (MΩ)	154	93	271	28	406	264	581	26	MW-test	0.0001
	Tau memb (ms)	12.0	6.5	20.6	28	25.8	20.2	37.3	25	MW-test	0.0003
AP properties	Threshold (mV)	-43.4	-47.0	-39.5	26	-44.0	-46.0	-41.3	26	T-test	0.7891
	Amplitude (mV)	65.2	54.6	70.3	25	69.0	62.8	73.4	25	T-test	0.1019
	Width (ms)	0.8	0.7	1.3	26	1.3	1.0	1.6	26	MW-test	0.0012

Median: quantile 50; Q1: quantile 25; Q3: quantile 75; n: number of cells; Vrest: Resting membrane potential; Ri : input resistance.